Mechanism of Acetylene Cyclotrimerization Catalyzed by the *fac*-IrP_3^+ Fragment: Relationship between Fluxionality and Catalysis

Claudio Bianchini,*,† Kenneth G. Caulton,*,‡ Catherine Chardon,§ Marie-Liesse Doublet,§ Odile Eisenstein,*,§ Sarah A. Jackson,§ Todd J. Johnson,‡ Andrea Meli,† Maurizio Peruzzini,† William E. Streib,‡ Alberto Vacca,† and Francesco Vizza†

Department of Chemistry and Molecular Structure Center, Indiana University, Bloomington, Indiana 47405, Istituto per lo Studio della Stereochimica ed Energetica dei Composti di Coordinazione, CNR, Via J. Nardi 39, 50132 Firenze, Italy, and Laboratoire de Chimie Théorique, Bâtiment 490, Université de Paris-Sud, 91405 Orsay, France

Received October 8, 1993®

Reaction of [(triphos)Ir(C_2H_4)$_2$](BPh$_4$) with C_2H_2 at 25 °C gives [(triphos)Ir(η^4-C_6H_6)](BPh$_4$), **1**, which was shown to have this Ir/benzene connectivity by single crystal X-ray diffraction. Crystal data (−155 °C): a = 16.471(6) Å, b = 17.126(6) Å, c = 12.030(4) Å, α = 101.22(2)°, β = 93.61(2)°, and γ = 75.46(1)° with Z = 2 in space group $P\bar{1}$. This species reacts with C_2H_2 in the presence of Cl^- to give (triphos)IrCl(η^2-C_4H_4), **2**, which can be converted back to **1** with C_2H_2 in the presence of the chloride scavenger $TlPF_6$. Ethyne will displace C_6H_6 from **1** at 60 °C in THF, thus completing a catalytic cyclotrimerization of C_2H_2 to benzene. While the phosphorus nuclei in **1** form an AM_2 spin system, these undergo site exchange with activation parameters $\Delta H^\ddagger$ = 10.7(3) kcal/mol and $\Delta S^\ddagger$ = −9.5(6) kcal^{-1} mol^{-1}. The benzene ring ^{1}H NMR spectra are also temperature-dependent, and the fluxionality can be accounted for by the same activation parameters appropriate to ^{31}P site exchange; the same physical mechanism thus accomplishes both site exchanges. The structural study indicates that η^4-C_6H_6, which is nonplanar, is a stronger π-acceptor than is butadiene itself. A multistep mechanism has been studied with extended Hückel calculations. It is shown that the C–C bond formation between the first two alkynes to give the unsaturated metallacyclopentadiene is permitted when the three spectator ligands are in a *fac* geometry but is forbidden when they are in a *mer* geometry, which explains the puzzling difference of reactivity between monodentate triphosphine and tripodal complexes. It is shown that this unsaturated metallacycle is highly reactive toward an incoming ligand since it is not strongly stabilized by conjugation within the π system. This explains why it can be isolated by trapping with a Lewis base. The addition of the third alkyne to the metallacyclopentadiene, leading to the η^4-benzene complex, can be achieved in a concerted manner and leads directly to the product. The C–C bond lengths within the η^4-benzene are shown to be due to the presence of a potent metal donor and to the nonplanarity of the benzene ring. The fluxionality of the η^4-benzene, which makes all carbons of the ring and the three phosphine ligands equivalent on the NMR time scale, is suggested to be due to an easy displacement/rotation of the IrP_3^+ fragment around the ring. This displacement avoids η^6-coordination (20-electron species) but passes through unsaturated η^3- and η^2-benzene coordination modes. These unsaturated species (notably the η^2 one) have the proper low-lying LUMO to coordinate an additional alkyne. This leads back to the monoalkyne complex and benzene production. Fluxionality and reactivity of the η^4-benzene ring are therefore interrelated. The efficiency of the catalysis is suggested to be due to the fact that all intermediates are reactive 16-electron species stabilized by additional donation from the conjugated π system of the organic ligand. The presence of an enforced *fac* arrangement of the three spectator ligands avoids the thermodynamic trap of the trigonal bipyramidal bis(alkyne) complex.

Introduction

The transition-metal catalyzed cyclotrimerization of alkynes is noteworthy as a process which forms three C–C bonds, yet it must stop there or run the risk of concurrently producing polyacetylene. It can be catalyzed by a wide variety of metals, oxidation states and d-electron configurations. It is undoubtedly the case that no single mechanism governs cyclotrimerization at all of these varied catalytic centers. The evidence for various mechanisms has been thoroughly reviewed by Wigley,[1] with particular reference to low-valent early (electropositive) transition metal centers.

We have reported[2] a series of studies where acetylene cyclotrimerization is effected at 25 °C by catalyst precursors containing the (triphos)Ir$^+$ substructure (triphos = MeC(CH_2PPh_2)$_3$). At the same time, we have reported on

† Istituto per lo Studio della Stereochimica ed Energetica dei Composti di Coordinazione.
‡ Indiana University.
§ Université de Paris-Sud.
® Abstract published in *Advance ACS Abstracts*, April 15, 1994.

(1) Smith, D. P.; Strickler, J. R.; Gray, S. D.; Bruck, M. A.; Holmes, R. S.; Wigley, D. E. *Organometallics* **1992**, *11*, 1275.
(2) Bianchini, C.; Meli, A.; Peruzzini, M.; Vacca, A.; Vizza, F. *Organometallics* **1991**, *10*, 645.

0276-7333/94/2313-2010$04.50/0

the structure, bonding, and reactivity of the $Ir(PMe_2Ph)_3^+$ moiety bound to alkynes, which shows no acetylene cyclotrimerization activity under the same conditions.[3] We report here a study of the structures and fluxionality of species derived from (triphos)M^{n+} with HC≡CH, together with a molecular orbital study of the likely individual steps in a cyclotrimerization mechanism.[4] This work shows the close relationship between those intramolecular migrations which lead to fluxionality and those which accomplish product (arene) release and return to the catalytic cycle by acetylene binding.

Experimental Section

General Information. All reactions and manipulations were routinely performed under nitrogen, unless otherwise stated, by using Schlenk techniques. Tetrahydrofuran (THF) was purified by distillation from $LiAlH_4$ under nitrogen. All other solvents and reagents were reagent grade and were used as received. Bis(triphenylphosphine)iminium chloride (PPNCl) was purchased from Aldrich. Literature methods were used for the preparation of [(triphos)$Ir(C_2H_4)_2$]BPh_4[5] and [(triphos)$IrCl(C_2H_4)$].[5] The solid complexes were collected on sintered-glass frits and washed with appropriate solvents before being dried under a stream of nitrogen. Infrared spectra were recorded on a Perkin-Elmer 1600 Series FTIR spectrophotometer using samples mulled in Nujol between KBr plates. ^1H and $^{31}P\{^1H\}$ NMR were recorded on either a Varian VXR 300 (299.94- and 121.42-MHz) or a Bruker ACP 200 (200.13- and 81.01-MHz) spectrometer. ^1H NMR shifts were measured relative to the residual ^1H NMR resonance in the deuterated solvent (CD_2Cl_2, δ 5.32; $CDCl_3$, δ 7.13). ^{31}P NMR shifts are relative to external 85% H_3PO_4 with downfield values reported as positive. $^{13}C\{^1H\}$ NMR spectra were recorded on the Bruker instrument operating at 50.32 MHz. Chemical shifts are relative to the deuterated solvent resonance (CD_2Cl_2, δ 53.1; $CDCl_3$, δ 77.7). Broad band and selective $^{31}P\{^1H\}$ NMR experiments were carried out on the Bruker ACP 200 instrument equipped with a 5-mm inverse probe and a BFX-5 amplifier. ^{13}C-DEPT, 2D-HETCOR, and 2D-COSY NMR experiments were run on the Bruker ACP 200 spectrometer. The computer simulation of NMR spectra was carried out with a locally-developed package containing the programs LAOCN3[6] and DAVINS,[7] running on a Compaq Deskpro 386/25 personal computer. The initial choices of shifts and coupling constants were refined by iterative least-squares calculations using the experimental digitized spectrum. The line-shape analysis of the variable-temperature NMR spectra was accomplished by means of the DNMR3 program[8] adapted for the Compaq computer. Errors in the calculated rate constants were estimated by varying the rate constant around the best-fit value, until an observable difference between simulated and experimental spectra, both displayed on the graphical terminal, could be detected. These errors proved to be 10% (only at the coalescence point) or less. Conductivities were measured with an Orion Model 990101 conductance cell connected to a Model 101 conductivity meter. The conductivity data were obtained at sample concentrations of *ca.* 10^{-3} M in nitroethane solutions at room temperature. GC analyses were performed on a Shimadzu GC-8A gas chromatograph fitted with a thermal conductivity detector and a 6-ft. 0.1% SP-1000 80/100 Carbopack C $^1/_8$-in. stainless steel column (Supelco Inc.). Quantification was achieved with a Shimadzu C-R6A Chromatopac coupled with the chromatograph, operating with an automatic correct area normalization method.

Synthesis of [(triphos)$Ir(\eta^4$-$C_6H_6)$]BPh_4 (1). A. [(triphos)$Ir(C_2H_4)_2$]BPh_4 (0.41 g, 0.34 mmol) was dissolved in THF (30 mL) under ethyne (1 atm) at room temperature. After 1 h, ethyne was replaced with nitrogen and the resulting orange solution was treated with ethanol (40 mL). On partial evaporation of the solvent, yellow crystals of 1 precipitated. They were filtered off and washed with *n*-pentane; yield 95%. Anal. Calcd for $C_{71}H_{65}BIrP_3$: C, 70.23; H, 5.40; Ir, 15.83. Found: C, 70.11; H, 5.36; Ir, 15.71. Λ_M = 48 $cm^2\ \Omega^{-1}\ mol^{-1}$. Spectral data have been reported.[4]

B. An equimolar mixture of [(triphos)$IrCl(C_2H_4)$] (0.30 g, 0.34 mmol) and $TlPF_6$ (0.12 g, 0.34 mmol) in THF (30 mL) was stirred at room temperature under ethyne (1 atm) for 2 h. After replacing ethyne with nitrogen, TlCl was removed by filtration. Addition of $NaBPh_4$ (0.17 g, 0.5 mmol) and *n*-heptane (60 mL) to the orange solution led to the precipitation of a yellow solid. Two recrystallizations from THF/ethanol/*n*-heptane gave pure samples of 1 in 65% yield.

Reaction of [(triphos)$Ir(\eta^4$-$C_6H_6)$]BPh_4 (1) with Ethyne. A THF (10 mL) solution of 1 (0.06 g, 0.05 mmol) was stirred under a 1-atm pressure of ethyne at 60 °C for 24 h. At regular intervals (*ca.* every 30 min), the reaction mixture was sampled and monitored by GC analysis, showing formation of benzene (0.5 mol of benzene/mol of catalyst/h). $^{31}P\{^1H\}$ NMR showed 1 to be the only phosphorus-containing compound present in solution during and at the end of the catalytic reaction. Compound 1 was quantitatively recovered at the end of the reaction. When the reaction was carried out at room temperature, no benzene production was observed.

Reaction of [(triphos)$Ir(\eta^4$-$C_6H_6)$]BPh_4 (1) with Ethyne in the Presence of PPNCl. A solution of 1 (0.30 g, 0.25 mmol) and PPNCl (0.14 g, 0.25 mmol) in THF (40 mL) was heated at reflux temperature under ethyne (1 atm). After 2 h, the resulting colorless solution was concentrated under reduced pressure to *ca.* 10 mL and the precipitated $PPNBPh_4$ eliminated by filtration. The filtrate, treated with *n*-heptane (30 mL), led to the precipitation of sandy crystals of [(triphos)$IrCl(\eta^2$-$C_4H_4)$] (2) in 80% yield. Anal. Calcd for $C_{45}H_{43}ClIrP_3$: C, 59.76; H, 4.79; Ir, 21.25. Found: C, 59.74; H, 4.72; Ir, 21.09.

Reaction of [(triphos)$IrCl(\eta^2$-$C_4H_4)$] (2) with Ethyne in the Presence of $TlPF_6$. A solid sample of 2 (0.30 g, 0.33 mmol) was added to a stirred THF (30-mL) solution of $TlPF_6$ (0.12 g, 0.34 mmol) under a steady stream of ethyne at room temperature. Within a few minutes, the solid dissolved to give an orange solution. After 1 h, TlCl was removed by filtration and then $NaBPh_4$ (0.17 g, 0.50 mmol) in ethanol (30 mL) was added. On partial evaporation of the solvent under a stream of nitrogen, yellow crystals of 1 precipitated in 80% yield.

Molecular Orbital Calculations. The extended Hückel calculations (EHT) were carried out by using the weighted H_{ij} formula.[9] The atomic parameters for Ir are taken from the literature.[3b] The geometries for the several model species were taken from the experimental data on related complexes: $P_3Ir(\eta^4$-$C_6H_6)^+$, this work; $P_3Ir(C_2R_2)^+$, ref 3b, $P_3Ir(C_4R_4)^+$, ref 10; $P_3Ir(C_5H_5)$, ref 11 (with the following changes: Ir–P = 2.3 Å, C–C = 1.4 Å in the benzene complex, P–Ir–P = 90°). For the planar benzene complex, Ir–(C_6H_6 plane) = 1.9 Å. The phosphines were modeled by PH_3.

X-ray Structure Determination of [(triphos)$Ir(C_6H_6)$]$BPh_4 \cdot {}^1/_2THF$. A crystal of suitable size was mounted in a nitrogen atmosphere glovebag using silicone grease and was transferred to a goniostat where it was cooled to −155 °C for characterization

(3) (a) Marinelli, G.; Rachidi, I. E.-I.; Streib, W. E.; Eisenstein, O.; Caulton, K. G. *J. Am. Chem. Soc.* **1989**, *111*, 2346. (b) Marinelli, G.; Streib, W. E.; Huffman, J. C.; Caulton, K. G.; Gagné, M. R.; Takats, J.; Dartiguenave, M.; Chardon, C.; Jackson, S. A.; Eisenstein, O. *Polyhedron* **1990**, *9*, 1867.

(4) Preliminary communication: Bianchini, C.; Caulton, K. G.; Chardon, C.; Eisenstein, O.; Folting, K.; Johnson, T. J.; Meli, A.; Peruzzini, M.; Rauscher, D. J.; Streib, W. E.; Vizza, F. *J. Am. Chem. Soc.* **1991**, *113*, 5127.

(5) Barbaro, P. L.; Bianchini, C.; Meli, A.; Peruzzini, M.; Vacca, A.; Vizza, F. *Organometallics* **1991**, *10*, 2227.

(6) Castellano, S.; Bothner-By, A. A. *J. Chem. Phys.* **1964**, *41*, 3863.

(7) Stephenson, D. S.; Binsch, G. *J. Magn. Reson.* **1980**, *37*, 395.

(8) Available from the Quantum Chemistry Program Exchange, Indiana University.

(9) Ammeter, J. H.; Bürgi, H.-B.; Thibeault, J. C.; Hoffmann, R. *J. Am. Chem. Soc.* **1978**, *100*, 3086.

(10) Thorn, D. L.; Hoffman, R. *Nouv. J. Chim.* **1979**, *3*, 39.

(11) Bleeke, J. R. *Acc. Chem. Res.* **1991**, *24*, 271.

Table 1. Crystallographic Data for [(triphos)IrC$_6$H$_6$]BPh$_4$·$^1/_2$THF

chemical formula	$C_{71}H_{65}BIrP_3 \cdot {}^1/_2THF$	space group	$P\bar{1}$
a, Å	16.471(6)	T, °C	−155
b, Å	17.126(6)	λ, Å	0.710 69
c, Å	12.030(4)	ρ_{calcd}, g cm^{-3}	1.252
α, deg	101.22(2)	μ(Mo Kα), cm^{-1}	21.7
β, deg	93.61(2)	R	0.0845
γ, deg	75.46(1)	R_w	0.0819
V, Å^3	3221.68		
Z	2		
fw	1214.25		

(Table 1) and data collection ($6° < 2\theta < 45°$).[12] A systematic search of a limited hemisphere of reciprocal space revealed no symmetry among the observed intensities. An initial choice of space group $P\bar{1}$ was later proven correct by the fact that attempted refinement in space group $P1$ was unsatisfactory. Following complete intensity data collection and correction for absorption, data processing gave a residual of 0.047 for the averaging of 911 unique intensities which had been measured more than once. Four standards measured every 400 data showed no significant trends. The structure was solved using a combination of direct methods (MULTAN78) and Fourier techniques. The Ir and P positions were determined from an initial E map and the remaining non-hydrogen atoms were obtained from subsequent iterations of least-squares refinement and difference Fourier calculation. One group of residual peaks that formed a five-membered ring was included as five half-weight carbons to model a partial-occupancy THF solvent molecule. The remaining residual peaks were rejected as being chemically unreasonable. The possibility of additional severely disordered solvent cannot be ruled out. Hydrogens were included in fixed calculated positions for all except the solvent atoms. The largest peak in the final difference map was 4.9 e/Å^3 in a cage formed by Ir(1), P(2), P(15), P(28), and C(41)–C(44). A false peak this large is somewhat unusual; however, a second data set collected on a crystal of different shape from a different sample gave the same result. Results of the structure determination are shown in Tables 2 and 3. Additional details are available as supplementary material.

Results

[(triphos)Ir(η^4-C$_6$H$_6$)]BPh$_4$ (1). When a steady stream of ethyne is passed at room temperature through a THF solution of either [(triphos)Ir(C$_2$H$_4$)$_2$]BPh$_4$ or [(triphos)-IrCl(C$_2$H$_4$)] in the presence of TlPF$_6$ as chloride scavenger, orange crystals of [(triphos)Ir(η^4-C$_6$H$_6$)]BPh$_4$ (1) are obtained in excellent yields by addition of ethanol/*n*-heptane, followed by slow evaporation of the solvent [triphos = MeC(CH$_2$PPh$_2$)$_3$]. Evolution of C$_2$H$_4$ was established by GC and ^{1}H NMR. Alternatively, 1 is synthesized in almost quantitative yield by treatment of the iridacyclopentadiene complex [(triphos)IrCl(η^2-C$_4$H$_4$)] (2) (see below) in THF with a stoichiometric amount of TlPF$_6$ under a steady stream of ethyne at room temperature, followed by NaBPh$_4$ addition in ethanol.

Complex 1 is stable in the solid state and in deaerated solutions, in which it behaves as a 1:1 electrolyte. The IR spectrum is featureless in the 2500–1500-cm^{-1} region where ν(Ir—H), ν(Ir—σ-C≡CH), ν(C=C), and ν(Ir—π-HC≡CH) are generally observed. The only remarkable new band is a weak one at 1605 cm^{-1} in the region of aromatic ν(C—C).

The variable-temperature ^{31}P{^{1}H} NMR spectra in CDCl$_3$ show 1 to be fluxional on the NMR time scale (Figure 1, left). In the fast exchange limit (>30 °C), the spectrum consists of an A$_3$ spin system (δ −22.75 at 40 °C), which transforms into an AM$_2$ pattern in the slow exchange limit (<0 °C) (δ(P$_A$) −27.13, δ(P$_M$) −19.56 at −60 °C) with an unusually small J(PP) (1.5 Hz). The mutual exchange mechanism that renders equivalent the three phosphorus atoms of triphos has been studied by spectral simulation,[13] assuming exchange between the three configurations $P_1P_2P_3 \rightleftharpoons P_3P_1P_2 \rightleftharpoons P_2P_3P_1$. A satisfactory simulation of the variable-temperature spectra (Figure 1, right) has been obtained by using T_2 = 0.12 s and the rate constants k shown in Figure 1. Plotting log k against $1/T$ results in a straight line (Figure 2). An Eyring plot yields the activation parameters ΔH^* (10.7 ± 0.2 kcal mol^{-1}), ΔS^* (−9.5 ± 0.6 cal K^{-1} mol^{-1}), and ΔG^*_{298K} (13.5 ± 0.04 kcal mol^{-1}). The negative but near-zero value for ΔS^* is consistent with the transition state for the fluxional process being intramolecular but ordered.

The variable-temperature ^{1}H NMR spectra of 1 in CDCl$_3$ are reported in Figure 3. The spectrum recorded at 50 °C shows a broad resonance at 5.18 ppm for the six hydrogens of the benzene ligand. At *ca.* 0 °C, this resonance decoalesces and, at lower temperature, emerges from the baseline to give three well-separated bands that at −40 °C fall at 6.49 ppm (partially masked by the resonances of the phenyl rings of triphos and BPh$_4^-$), 5.86 ppm (2H), and 3.16 ppm (2H). Even at the lowest temperature attained (−100 °C in CD$_2$Cl$_2$), the three resonances show no well-resolved H–H couplings. However, from selective decoupling experiments as well as a H,H-COSY experiment, it is evident that the band at 3.16 ppm is correlated to the other two, which are not correlated with each other. This finding allows us to assign the highest field resonance to the central Ir—C—H hydrogens (H$_B$) and the lowest field resonance to the hydrogen atoms of the uncoordinated HC=CH moiety (H$_A$)

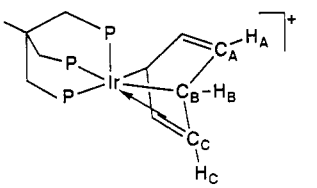

A rough evaluation of the coupling interaction between the three different pairs of hydrogens can be obtained by selective homodecoupling experiments by measuring the decrease in line width ($w_{1/2}$) upon crossover irradiation of the three signals. In particular upon irradiation of the H$_B$ signal, the $w_{1/2}$ values of the resonances due to H$_A$ and H$_C$ decrease by *ca.* 4 and 3 Hz, respectively. No variation of the peak width is observed when the resonances due to H$_A$ and H$_C$ are selectively decoupled. An unambiguous computer simulation of the ^{1}H NMR spectra cannot be provided, as it is not possible to carry out a line-shape analysis. The spin system is, in fact, extremely complicated (AA′BB′CC′XX′Y). However, by using a simplified ABCX model and introducing the rate constants calculated from the activation parameters obtained from the temperature-dependent ^{31}P NMR spectra, we have been able to reproduce the variable-temperature experimental spectra. The exchange mechanism is ABC ⇌ BCA ⇌ CAB with the following coupling constants: J(AB) = 4 Hz, J(BC)

(12) For general data collection and processing procedures, see: Huffman, J. C.; Lewis, L. N.; Caulton, K. G. *Inorg. Chem.* **1980**, *19*, 2755.

(13) Kleier, D. A.; Binsch, G. A Computer Program for the Calculation of Complex Exchange-Broadened NMR Spectra. QCPE Program No. 165; Indiana University: Bloomington, IN.

Table 2. Fractional Coordinates and Isotropic Thermal Parameters[a] for [(triphos)IrC$_6$H$_6$]BPh$_4$·$^1/_2$THF

	10^4x	10^4y	10^4z	$10B_{iso}$ (Å^2)		10^4x	10^4y	10^4z	$10B_{iso}$ (Å^2)
Ir(1)	6176.9(4)	3223.0(4)	2389(1)	25	C(42)	8054(9)	2296(9)	3501(12)	28
P(2)	6166(2)	2840(2)	4128(3)	27	C(43)	6846(9)	1807(9)	4135(13)	30
C(3)	5148(9)	2823(8)	4671(11)	25	C(44)	7418(9)	1257(9)	2133(13)	31
C(4)	4981(10)	2118(10)	4951(13)	37	C(45)	8259(10)	873(9)	3830(14)	37
C(5)	4226(11)	2177(10)	5453(13)	37	C(46)	5831(13)	3759(12)	828(17)	57
C(6)	3638(11)	2911(11)	5683(13)	41	C(47)	5064(14)	3616(12)	1272(18)	62
C(7)	3801(9)	3595(10)	5415(13)	35	C(48)	4903(10)	3997(12)	2371(16)	52
C(8)	4549(9)	3553(9)	4927(13)	31	C(49)	5494(14)	4515(9)	2853(15)	54
C(9)	6499(9)	3482(8)	5391(11)	26	C(50)	5711(15)	4956(16)	2077(20)	76
C(10)	6712(9)	4213(8)	5322(12)	27	C(51)	5863(14)	4565(15)	983(21)	69
C(11)	6953(10)	4676(9)	6308(13)	37	B(52)	1340(10)	1690(9)	4445(13)	24
C(12)	6984(11)	4437(10)	7342(13)	39	C(53)	2210(8)	1188(7)	4970(11)	20
C(13)	6753(12)	3730(11)	7423(14)	45	C(54)	2375(9)	1245(8)	6149(12)	26
C(14)	6535(11)	3250(9)	6426(13)	37	C(55)	3122(10)	790(9)	6568(13)	34
P(15)	6462(2)	1845(2)	1553(3)	25	C(56)	3748(9)	271(8)	5839(13)	30
C(16)	6580(9)	1594(8)	19(12)	29	C(57)	3589(9)	224(9)	4671(12)	30
C(17)	7316(10)	1209(11)	−516(14)	44	C(58)	2857(9)	662(9)	4271(11)	28
C(18)	7387(13)	1036(13)	−1672(16)	56	C(59)	949(9)	1020(8)	3586(12)	25
C(19)	6695(13)	1298(9)	−2337(14)	44	C(60)	783(9)	342(8)	3937(12)	28
C(20)	5933(12)	1684(11)	−1849(12)	42	C(61)	486(10)	−280(9)	3217(14)	38
C(21)	5884(10)	1818(11)	−646(13)	39	C(62)	321(12)	−219(11)	2068(15)	47
C(22)	5666(8)	1289(8)	1689(11)	22	C(63)	479(12)	424(11)	1675(14)	51
C(23)	5844(9)	440(9)	1339(11)	27	C(64)	771(12)	1041(11)	2415(14)	46
C(24)	5234(10)	7(9)	1396(12)	30	C(65)	656(8)	2201(8)	5428(11)	23
C(25)	4463(9)	388(10)	1781(12)	32	C(66)	−135(9)	2067(9)	5539(11)	27
C(26)	4272(9)	1230(10)	2156(14)	40	C(67)	−736(10)	2569(10)	6324(12)	34
C(27)	4887(10)	1671(9)	2097(13)	35	C(68)	−536(10)	3235(9)	7054(12)	33
P(28)	7616(2)	3082(2)	2633(3)	26	C(69)	253(10)	3367(9)	6992(12)	33
C(29)	8055(9)	3946(8)	3324(12)	27	C(70)	825(10)	2856(9)	6209(12)	30
C(30)	8576(10)	3926(9)	4271(13)	32	C(71)	1489(9)	2408(8)	3800(11)	26
C(31)	8884(10)	4615(9)	4717(13)	35	C(72)	2278(9)	2518(8)	3612(12)	27
C(32)	8714(10)	5283(8)	4253(13)	32	C(73)	2357(10)	3153(10)	3068(14)	37
C(33)	8222(10)	5303(9)	3291(14)	33	C(74)	1682(12)	3667(10)	2728(12)	39
C(34)	7875(10)	4641(9)	2789(13)	36	C(75)	871(10)	3604(10)	2924(14)	38
C(35)	8242(9)	2786(8)	1328(12)	25	C(76)	804(10)	2976(9)	3450(13)	34
C(36)	7932(12)	2909(15)	302(17)	63	C(77)	1579(20)	1140(19)	8912(33)	45
C(37)	8444(12)	2720(15)	−652(15)	60	C(78)	2102(26)	660(22)	9512(30)	53
C(38)	9255(11)	2428(10)	−568(13)	38	C(79)	2375(26)	1151(25)	10444(26)	58
C(39)	9597(13)	2284(20)	448(17)	98	C(80)	2336(42)	1852(30)	10114(48)	118
C(40)	9066(14)	2480(19)	1392(15)	92	C(81)	1776(28)	1970(22)	9213(32)	55
C(41)	7611(10)	1588(10)	3371(13)	38					

[a] Isotropic values for those atoms refined anisotropically are calculated using the formula given by: Hamilton, W. C. *Acta Crystallogr.* **1959**, *12*, 609.

Table 3. Selected Bond Distances (Å) and Angles (deg) for [(triphos)Ir(C$_6$H$_6$)]BPh$_4$·$^1/_2$THF

Ir(1)–P(2)	2.313(4)	C(46)–C(47)	1.494(28)
Ir(1)–P(15)	2.319(4)	C(46)–C(51)	1.372(28)
Ir(1)–P(28)	2.327(4)	C(47)–C(48)	1.367(26)
Ir(1)–C(46)	2.229(20)	C(48)–C(49)	1.493(27)
Ir(1)–C(47)	2.245(22)	C(49)–C(50)	1.42(3)
Ir(1)–C(48)	2.184(15)	C(50)–C(51)	1.36(3)
Ir(1)–C(49)	2.196(16)		
P(2)–Ir(1)–P(15)	88.55(13)	C(47)–Ir(1)–C(48)	35.9(7)
P(2)–Ir(1)–P(28)	88.25(14)	C(47)–Ir(1)–C(49)	65.2(7)
P(2)–Ir(1)–C(46)	164.6(5)	C(48)–Ir(1)–C(49)	39.9(7)
P(2)–Ir(1)–C(47)	127.0(6)	Ir(1)–C(46)–C(47)	71.1(12)
P(2)–Ir(1)–C(48)	99.2(5)	Ir(1)–C(46)–C(51)	112.9(16)
P(2)–Ir(1)–C(49)	98.7(5)	C(47)–C(46)–C(51)	115.2(18)
P(15)–I(28)–P(28)	88.04(13)	Ir(1)–C(47)–C(46)	69.9(12)
P(15)–Ir(1)–C(46)	98.5(5)	Ir(1)–C(47)–C(48)	69.6(11)
P(15)–Ir(1)–C(47)	95.4(5)	C(46)–C(47)–C(48)	113.0(17)
P(15)–Ir(1)–C(48)	120.6(6)	Ir(1)–C(48)–C(47)	74.5(12)
P(15)–Ir(1)–C(49)	159.8(5)	Ir(1)–C(48)–C(49)	70.5(9)
P(28)–Ir(1)–C(46)	105.6(5)	C(47)–C(48)–C(49)	113.5(17)
P(28)–Ir(1)–C(47)	144.6(6)	Ir(1)–C(49)–C(48)	69.6(8)
P(28)–Ir(1)–C(48)	150.4(6)	Ir(1)–C(49)–C(50)	108.2(15)
P(28)–Ir(1)–C(49)	110.8(6)	C(48)–C(49)–C(50)	113.9(16)
C(46)–Ir(1)–C(47)	39.0(7)	C(49)–C(50)–C(51)	118.2(21)
C(46)–Ir(1)–C(48)	65.5(7)	C(46)–C(51)–C(50)	111.9(22)
C(46)–Ir(1)–C(49)	70.3(7)		

= 2 Hz, J(BX) = 6 Hz. The second-order effects that broaden the resonances in the slow exchange region have been artifically reproduced by introducing a very low value of T_2 (0.06 s). In contrast, in the fast exchange region where second-order effects are expected to disappear, a more realistic T_2 value (0.3 s) has been introduced. In the range 233–303 K, a reasonable agreement between experimental and computed spectra (Figure 4) has been found. *Since a single set of activation parameters successfully accounts for the dynamic line shapes in both ^{31}P and ^1H NMR spectra, we conclude that a single mechanism accomplishes both site exchange processes.*

The $^{13}C\{^1H\}$ NMR spectrum of **1** (CD_2Cl_2, −50 °C) exhibits three resonances at δ *ca.* 132 (masked by phenyl carbon atoms), δ 86.77 (brd, J(CP) = 6.7 Hz), and δ 55.31 (dd, J(CP) = 38.7, 6.2 Hz). When the temperature is raised, the resonances broaden and, at *ca.* 20 °C, merge into the baseline. On the basis of the C–P coupling constant values and, in particular, of a ^{13}C–^1H heteronuclear 2D-NMR correlation study in CD_2Cl_2 at −50 °C (Figure 5), the three resonances were readily assigned to the C_C, C_A, and C_B carbon atoms, respectively.

Reaction of **1** with ethyne in THF at 60 °C shows (GC) production of benzene at a rate of 0.5 mol of benzene (mol of catalyst)$^{-1}$ h^{-1}, over a 24-h period. When the reaction was carried out in the presence of PPNCl, no catalytic process occurred, since the 16-electron intermediate [(triphos)Ir(η^2-C$_4$H$_4$)]$^+$ is trapped by chloride to give [(triphos)IrCl(η^2-C$_4$H$_4$)] (**2**) which is stable under catalytic

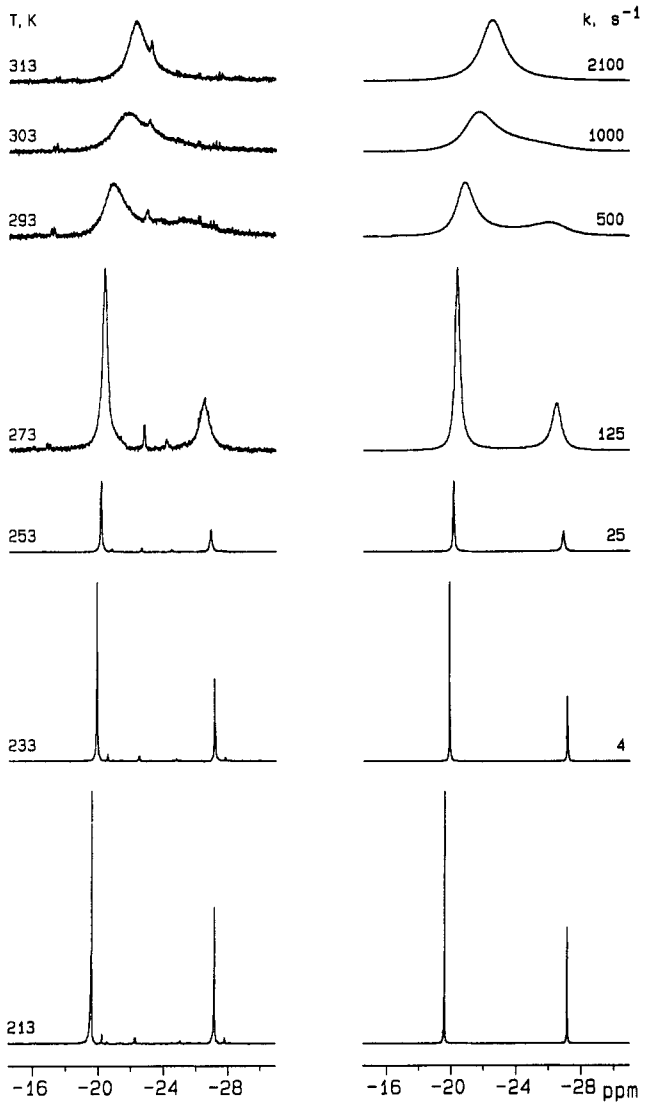

Figure 1. Experimental (left) and computed (right) variable-temperature $^{31}P\{^1H\}$ NMR spectra of 1 ($CDCl_3$, 121.42 MHz). The intensities of the spectra at 273, 293, 303, and 313 K are purposefully increased by 10 times.

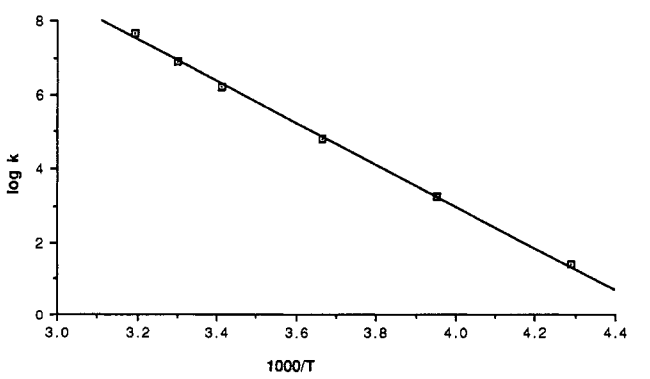

Figure 2. Arrhenius plot for the rate constants obtained from the computer simulation of the variable-temperature $^{31}P\{^1H\}$ NMR spectra of 1.

conditions. However, addition of $TlPF_6$ and ethyne in THF regenerates the catalytically active 1.

[(triphos)IrCl(η^2-C_4H_4)] (2). The complex behaves as a nonelectrolyte in CH_2Cl_2 and $EtNO_2$. The $^{31}P\{^1H\}$ NMR spectrum in CD_2Cl_2 is temperature-invariant in the range +20 to −90 °C and consists of a first-order AM_2 spin system (20 °C: $\delta(P_A)$ −27.26, $\delta(P_M)$ −39.96, $J(PP)$ = 15.9 Hz). This pattern is typical of octahedral triphos metal complexes containing two chemically-equivalent phosphorus nuclei. The ^1H NMR spectrum (CD_2Cl_2, 20 °C) exhibits a multiplet at δ 6.45 (Figure 6b) readily attributable to the two β-hydrogens of a C_4H_4 diene ligand.[2] An H,H-COSY experiment shows this resonance to be correlated with a resonance at *ca.* 7.5 ppm (α-hydrogens) masked by the signals of the phenyl hydrogens. The higher field signal has been simulated (Figure 6a) as the AA′ part of an AA′MM′XX′Y spin system with the following parameters (X, X′, and Y denote the phosphorus atoms of triphos): $^3J(AA')$ = 4.5 Hz, $^3J(AM)$ = 8.5 Hz, $^4J(AM')$ = 1.0 Hz, $^4J(AX)$ = 11.6 Hz, $^4J(AX')$ = 1.2 Hz, $^4J(AY)$ = −1.0 Hz, $^4J(MM')$ = 6.8 Hz, $^2J(XX')$ = 1.5 Hz).

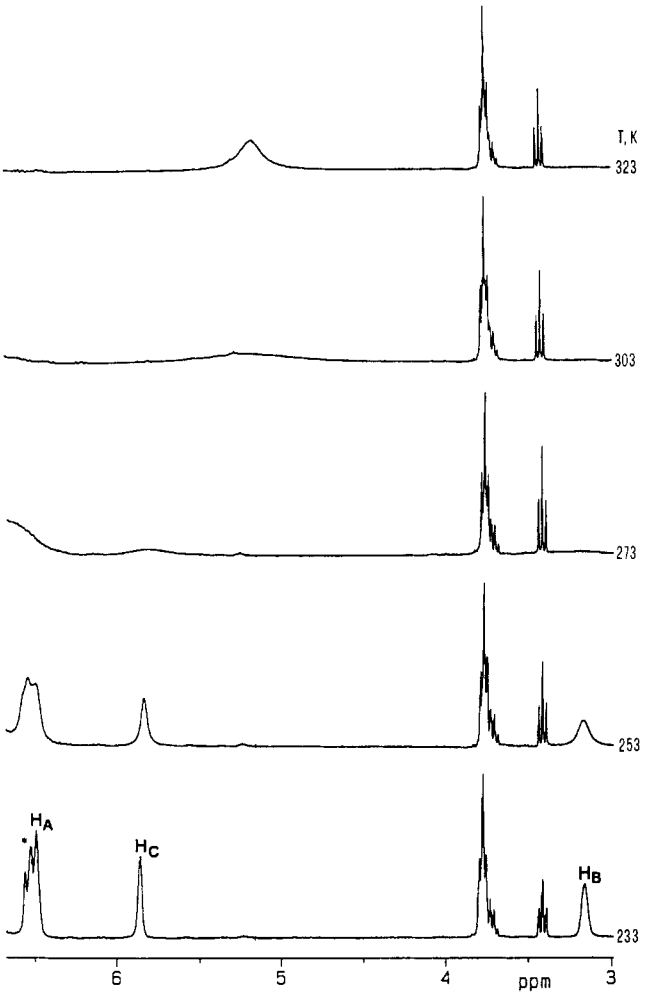

Figure 3. Experimental variable-temperature ^1H NMR spectra of 1 in the 7–3 ppm region ($CDCl_3$, 299.95 MHz). The asterisk refers to aromatic protons.

The $^{13}C\{^1H\}$ NMR spectrum of **2** (CD_2Cl_2, 20 °C) exhibits a single resonance at 153.72 ppm for the α-carbons of the C_4H_4 moiety, showing they are chemically (but not magnetically) equivalent. This resonance consists of a ddd pattern and has been simulated as the AA′ part of an AA′MM′Q spin system where M and M′denote the two phosphorus atoms trans to the C_4H_4 ligand and Q denotes the remaining phosphorus atom. The different values of $^2J(C_\alpha P)$ confirm the magnetic inequivalence of the phosphorus nuclei in **2** ($^2J(C_\alpha P_M)$ = 95.4 Hz, $^2J(C_\alpha P_{M'})$ = 9.3 Hz, $^2J(C_\alpha P_Q)$ = 7.4 Hz). The resonance of the β-carbons of the C_4H_4 ligand falls at higher field, 142.36 ppm, and appears as a triplet ($^3J(C_\beta P)$ = 5.0 Hz). From a comparison of the spectroscopic data of **2** with those of the rhodium

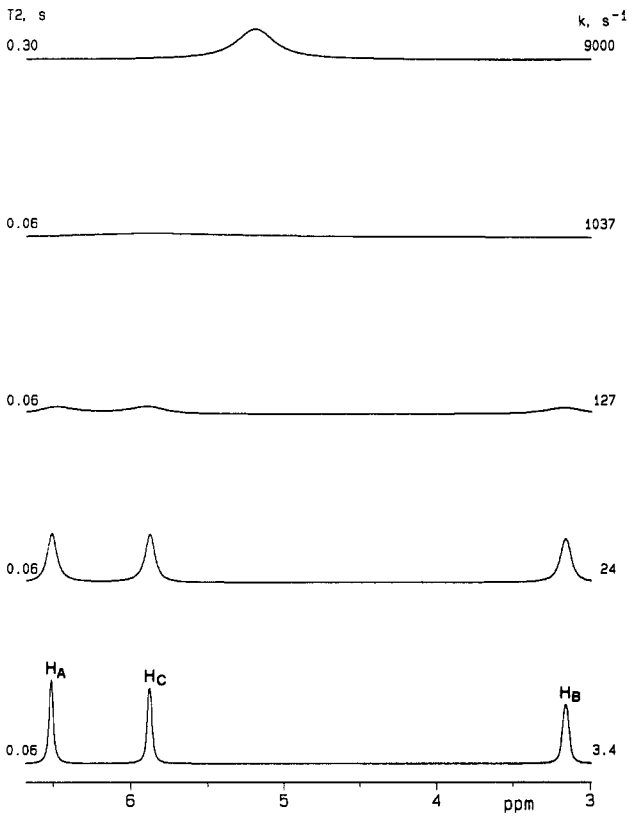

Figure 4. Computed variable-temperature ^{1}H NMR spectra of 1 in the 7–3 ppm region ($CDCl_3$, 299.95 MHz). The rate constants are calculated using the activation parameters obtained from the variable-temperature ^{31}P NMR spectra.

derivative [(triphos)RhCl(η^2-C_4H_4)] authenticated by an X-ray analysis,[4] one may readily infer that the two compounds share the same primary geometry; i.e., the metal center is octahedrally coordinated by triphos, by the two terminal carbons of a C_4H_4 diene moiety, and by a chloride ligand.

Solid-State Structure of [(triphos)Ir(η^4-C_6H_6)]-BPh_4·$^1/_2$THF. This salt contains noninteracting BPh_4^- and (triphos)Ir(η^4-C_6H_6)$^+$ ions, with THF filling holes in the lattice. The cation (Figure 7) has pseudomirror symmetry, with the mirror plane containing the Ir–P(28) bond and bisecting the C(47)–C(48) and C(50)–C(51) bonds. While the P–Ir–P angles are identical at 88°, the Ir–P(28) bond length (2.327(4) Å) is 3σ longer than the other two Ir–P distances (2.313(4) and 2.319(4) Å). This is consistent with a square-pyramidal structure with one of the Ir–P bonds as the apical group. While the four Ir–C bond lengths (**3**) show some distortions from mirror sym-

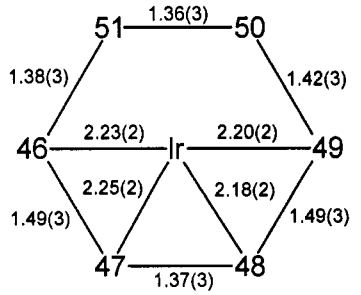

3

metry, these deviations do not exceed 2.5σ and are thus not statistically significant. The pattern of C(46)–C(47), C(47)–C(48), and C(48)–C(49) bond lengths (while just significant at the 3σ level) is long–short–long, consistent with extensive back-bonding.[14] In fact, they resemble the degree of back-bonding from low-valent *early* (i.e., electropositive) transition metals[15] to butadiene much more than late transition metal butadiene compounds. However, this long–short–long pattern is *generally* observed for η^4-arene compounds (which involve mainly late transition metals). The conclusion is that an η^4-arene is a much stronger *π-acceptor* than is butadiene itself.

In order to avoid repulsion between filled C=C and metal orbitals, the benzene folds about the C(46)/C(49) line to a dihedral angle of 134.8°.[16] Such bending must be considered as contributing to the π-acceptor capacity of η^4-benzene. This folding moves C(50) and C(51) beyond 2.97 Å from iridium.

Summary of Experimental Conclusions. Our experimental results suggest that the catalytic cycle (Figure 8) which has long been suggested is operating in our Ir(tripod)$^+$ system. The following points have been proven: (i) The η^4-benzene complex produces benzene in a catalytic manner upon ethyne addition; the catalytic cycle is stopped by Cl^- ([PPN]Cl) and restarts if Cl^- is removed by adding $TlPF_6$. (ii) A fluxional mechanism, which does not dissociate phosphines or benzene, makes all carbon and phosphorus atoms equivalent in **1**. Fluxionality and the cyclotrimerization reactions occur at the same temperature. (iii) From previous studies, we have learned that IrP_3(alkyne)$^+$ (P = monodentate phosphine) is an isolable species, suggesting that the corresponding complex with tripodal phosphine is a viable intermediate. The complex with monodentate phosphine and tripodal phosphine differ by another important point. The complex with monodentate phosphine produces a *cis*-bis(alkyne) trigonal bipyramidal complex with additional alkyne, and the two coordinated alkynes do not couple to make a metallacyclopentadiene. This suggests that the dialkyne complex with a *planar* MP_3 unit is a thermodynamically-stable dead-end channel for the catalytic reaction.

In order to understand better the several aspects of this reaction, we have studied the reaction path with extended Hückel (EHT) calculations.

Molecular Orbital Study of the Alkyne Cyclotrimerization. The few relevant, previous theoretical studies are limited to only selected parts of the pathway. The coupling of two alkynes linked to a CpCo fragment was investigated via *ab initio* calculations and the orientation favoring the formation of the C–C bond was determined.[17a] In the same study, the structure of the unsaturated species, $CpCo(C_4H_4)$, was optimized and was shown to be pyramidal at the Co center, which is in agreement with a previous MO analysis of d^6 $CpML_2$ complexes.[17b] In a preliminary communication,[4] we demonstrated that the addition of an alkyne to a $P_3Ir(C_4H_4)^+$ intermediate, facilitated by the match in symmetry between the frontier orbitals of

(14) The long C(49)–C(50) bond length and the higher esd's associated with C(50) arise from the larger (by 30%) thermal parameter of C(50). Some disorder of this carbon is indicated, in spite of the low temperature of the data collection.

(15) Erker, G.; Krüger, C.; Müller, G. *Adv. Organomet. Chem.* **1985**, *24*, 1. Yasuda, H.; Nakamura, A. *Angew. Chem., Int. Ed. Engl.* **1987**, *26*, 723.

(16) C(46)–C(49) are planar to within ±0.02 Å, as are C(49), C(50), C(51), and C(46).

(17) (a) Wakatsuki, Y.; Nomura, O.; Kitaura, K.; Morokuma, K.; Yamazaki, H. *J. Am. Chem. Soc.* **1983**, *105*, 1907. (b) Hoffman, P. *Angew. Chem., Int. Ed. Engl.* **1977**, *8*, 536.

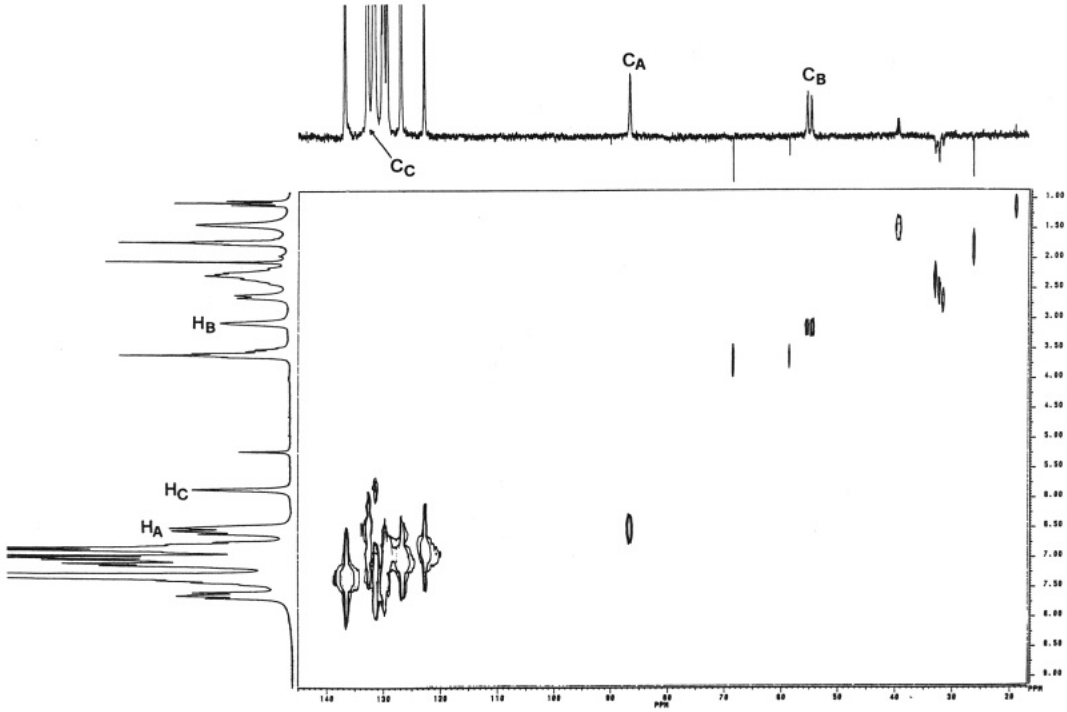

Figure 5. ^{13}C-^{1}H heteronuclear 2D-NMR correlation study of **1** in CD_2Cl_2 at −50 °C. The trace at the right shows a DEPT experiment for separation of CH_2 (negative) from CH and CH_3 carbon atoms (positive).

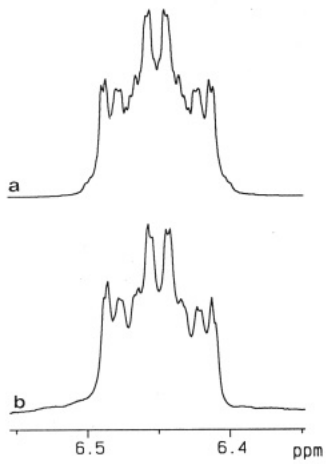

Figure 6. Experimental (*b*) and computed (*a*) ^{1}H NMR spectrum of the β-hydrogens of the β-C_4H_4 diene ligand in **2** (CD_2Cl_2, 200.13 MHz).

the two reactants leads, in a concerted manner, to the formation of $P_3Ir(\eta^4\text{-benzene})^+$.

Formation of Metallacyclopentadiene. A. Reactivity of *mer*- and *fac*-$P_3Ir(alkyne)^+$.[18] The monoalkyne complex $P_3Ir(alkyne)^+$ (P = PMe_2Ph) does not assume the classical planar structure expected for d^8 ML_4 complexes, preferring instead a geometry which is intermediate between a tetrahedron and a square pyramid, (**4**).[3] It has

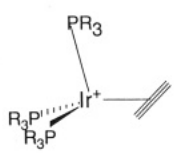

4

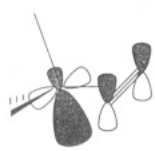

5

been shown that this structure is due to the tendency of the alkyne to donate more than 2 electrons to the metal which means that $P_3Ir(alkyne)^+$ is intermediate between a 16- and an 18-electron system. The fact that the complex is not fully saturated is confirmed by its high reactivity toward any incoming nucleophile[3] and supported by the presence of a low-lying LUMO pointing toward the vacant site, as shown in **5**. In the specific case where the incoming nucleophile is an alkyne, two types of reactions are observed: (i) addition of the alkyne, leading to the formation of a bis(alkyne) complex, and (ii) coupling of the alkynes, leading to the unsaturated metallacycle.

The addition reaction (i) has been observed for monodentate phosphines and dicarbomethoxyalkyne.[3b] The two alkynes occupy the equatorial sites of the trigonal bipyramid, **6**, and the three phosphines move from the *fac*

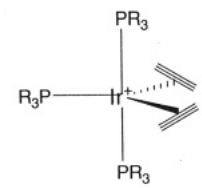

6

geometry in **4**, to a *mer* arrangement, a reorganization which is only possible for monodentate phosphines. The coupling reaction (ii) occurs only for tripodal phosphines (where the *fac* arrangement is constrained), for Ir(I) or Rh(I), and leads to the formation of a metallacyclopentadiene. In the case of Rh, this intermediate has been trapped using Cl^-. A similar reaction is believed to take place during the cyclotrimerization with CpCo (where the Cp group mimics three *fac* ligands).[19]

This intriguing difference in product identity from the *mer*- and *fac*-P_3Ir^+ fragments (monodentate and tripodal

(18) We use the term *fac* to indicate a pyramidal P_3M structure and *mer* to indicate a planar P_3M structure.

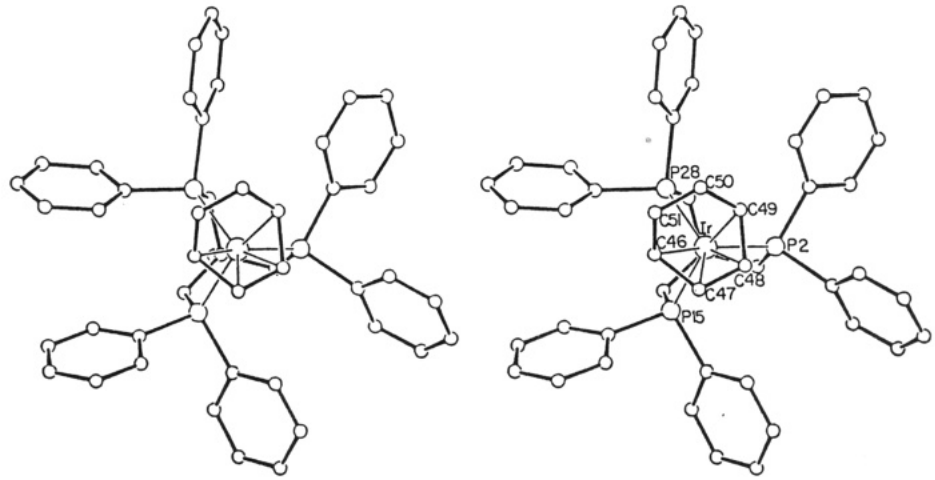

Figure 7. Stereo ORTEP drawing of the non-hydrogen atoms of (triphos)Ir(η^4-C_6H_6)$^+$, showing selected atom labeling.

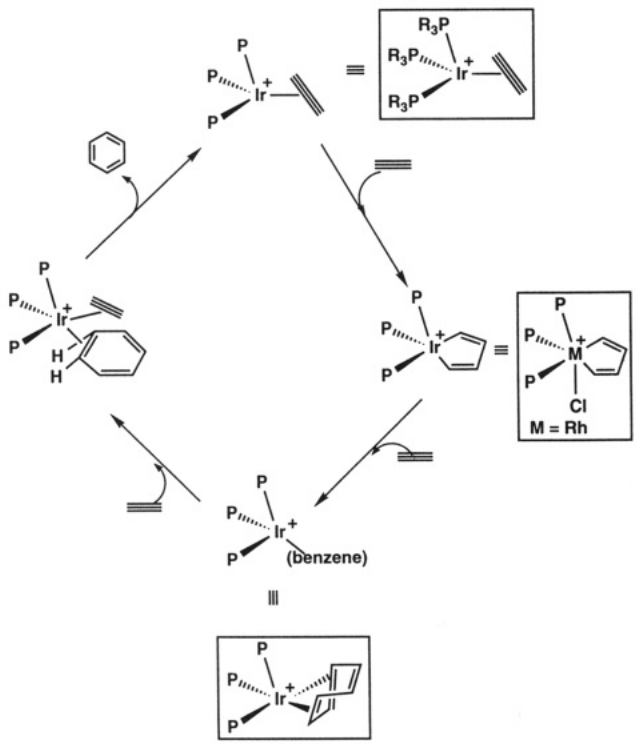

Figure 8. Representation of the catalytic reaction path for alkyne cyclotrimerization. The species which have been isolated and characterized by X-ray diffraction are indicated in boxes.

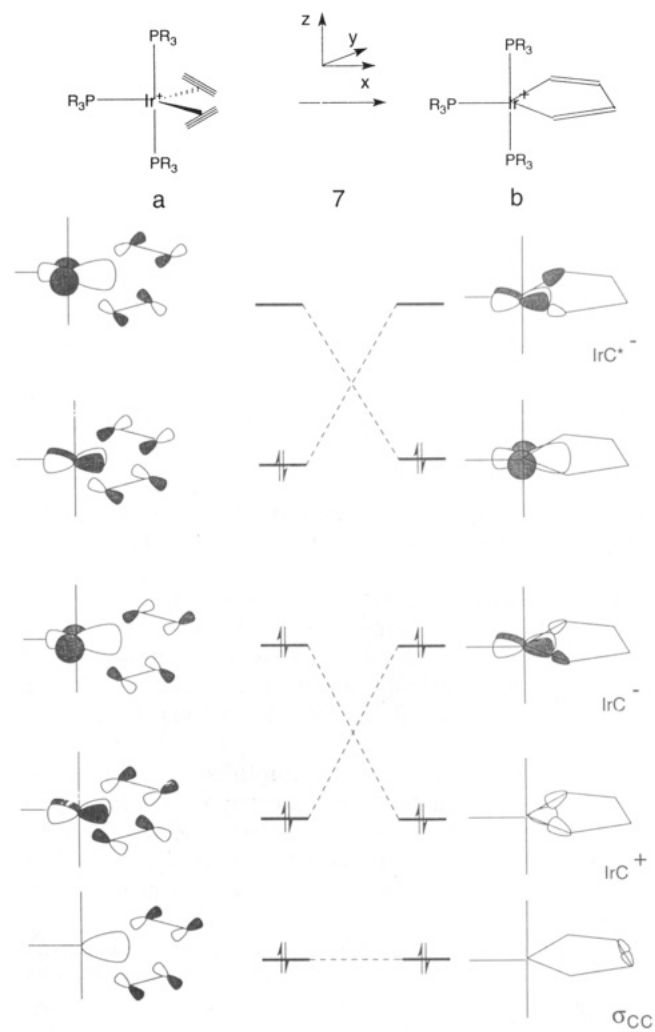

Figure 9. Simplified correlation diagram for C–C coupling in *mer*-$(PH_3)_3Ir(C_2H_2)_2^+$, preserving C_{2v} symmetry.

phosphines, respectively) needs to be explained. The most stable structure for a d^8 $ML_3L'_2$ (L′ = π-acceptor ligand) species is a trigonal bipyramid with the two L′ ligands lying in the equatorial plane.[3b,20] There is a strong preference for this structure, especially with the heavy metal center and the absence of ancillary π-acceptor ligands. This strong structural preference is supported by the lack of fluxional behavior in $P_3Ir(alkyne)_2^+$.[20] The complex adopts this structure if the three L ligands can adopt a *mer* arrangement, as is possible only for monodentate L.

We have constructed the correlation diagram (using the *xz* plane which bisects the incipient C–C bond as the symmetry element) for the coupling reaction, **7**, transforming the trigonal bipyramid into the metallacyclobutadiene and have found that this transformation is symmetry-forbidden (Figure 9). The correlation diagram is similar to that published by Hoffmann *et al.* for the coupling of two olefins in the same type of metallic system[21] and the presence of the additional alkyne π orbitals ($\pi_\perp$)

(19) (a) McAllister, D. R.; Bercaw, J. E.; Bergman, R. G. *J. Am. Chem. Soc.* **1977**, *99*, 1666. (b) Bönneman, H. *Angew. Chem., Int. Ed. Engl.* **1985**, *24*, 248. (c) Vollhardt, K. P. C. *Angew. Chem., Int. Ed. Engl.* **1984**, *23*, 539. (d) Gleiter, R.; Kratz, D. *Angew. Chem., Int. Ed. Engl.* **1990**, *29*, 276.

(20) Lundquist, E. G.; Folting, K.; Streib, W. E.; Huffman, J. C.; Eisenstein, O.; Caulton, K. G. *J. Am. Chem. Soc.* **1990**, *112*, 855.

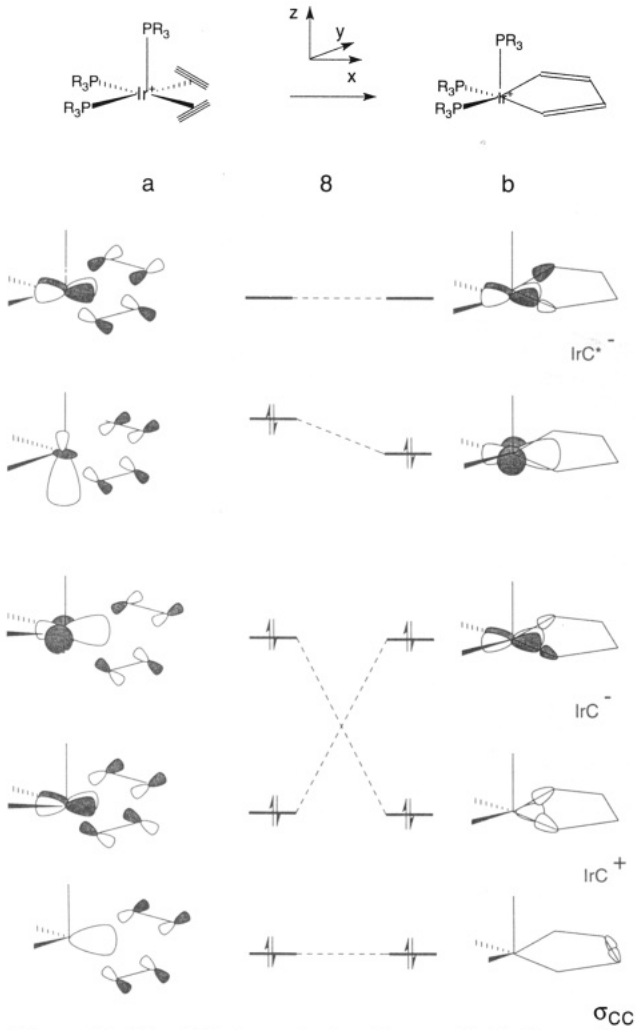

Figure 10. Simplified correlation diagram for C–C coupling in *fac*-$(PH_3)_3Ir(C_2H_2)_2^+$, preserving C_s symmetry.

does not modify its general shape. The same transformation becomes allowed when the two alkynes are attached to the *fac*-P_3Ir^+ fragment, as in Figure 10, in agreement with Morokuma's calculations[17a] which demonstrated that the reaction is also allowed for the isolobal CpCo fragment.[22]

Figures 9 and 10 show a simplified version of the correlation diagrams for molecular orbitals which are lying in the horizontal xy plane. The other molecular orbitals, perpendicular to the xy plane, do not vary significantly in energy along the reaction path and correlate in an allowed manner.

In both geometries, **7a** and **8a**, the three lowest orbitals shown correlate with bonding orbitals of the metallacycle (σ_{cc}, IrC^+, IrC^-). The difference between the two geometries comes from the xy orbital, which correlates with the empty orbital IrC^{*-} (the out-of-phase combination of the two Ir–C σ^* antibonding orbitals). The metal xy orbital is occupied in the trigonal bipyramid case, **7a**, and the coupling reaction is thus forbidden. It is empty in the square-based pyramid **8a**, and the reaction is allowed. In the latter structure, **8a**, the HOMO is the lone pair at the metal, destabilized by the five surrounding ligands. It

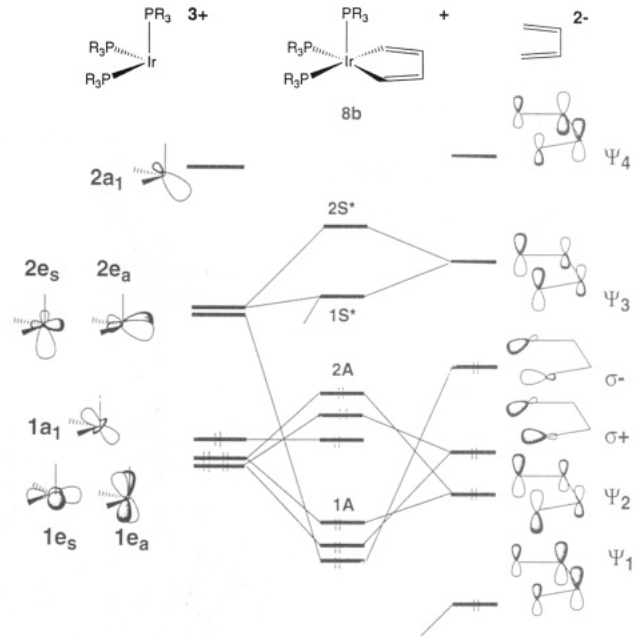

Figure 11. Orbital diagram for *fac*-$(PH_3)_3Ir(C_4H_4)^+$ as made from $(PH_3)_3Ir^{3+}$ and $C_4H_4^{2-}$.

correlates in an allowed way with x^2-y^2 of the metallacycle. This coupling reaction, which oxidizes the metal from d^8 to d^6 and forms a C–C bond, is allowed if the metal can provide an extra orbital of the same symmetry as the σ_{cc} bond (i.e., symmetrical with respect to the xz plane). This is the case for **8a** but not for **7a**.

This analysis of the first step in the mechanism of Figure 8 suggests that the C–C coupling reaction is favored by preventing the bis(alkyne) complex from falling into the thermodynamic trap represented by a trigonal bipyramidal structure. Tripodal phosphines and Cp groups thus serve this function.

B. Structure of the Metallacyclopentadiene. The structure of the unsaturated metallacyclopentadiene, **8b**, is unknown but may be inferred from the X-ray structure of the trapped product, [(triphos)RhCl(η^4-C_4H_4)],[4] where the metallacyclopentadiene ring is planar. Test calculations on the unsaturated species show that the planar ring is also preferred.[23a] This contrasts with the metallacyclopentadiene intermediates involved in the Dötz mechanism.[23b]

The construction of the molecular orbitals of **8b** from the $[IrP_3]^{3+}$ and $[C_4H_4]^{2-}$ fragments is given in Figure 11. The idealized P_3Ir^{3+} fragment has C_{3v} symmetry, and this group's symmetry labels are used for the fragment orbitals although the metallacycle has C_s symmetry.[24] The two Ir–C σ bonds result from the two bonding interactions between the empty metal fragment orbitals, $2a_1$ and $2e_a$, and the two symmetry-adapted combinations, σ^+ and σ^-, respectively, of the carbon σ lone pairs. A π-type interaction between the metal and the ring results from the stabilization of the low-lying ψ_1 by the empty $2e_s$, but this interaction is very weak because $2e_s$ overlaps weakly with ψ_1 (0.06) and because there is a large energy gap. The back-bonding from $1e_a$ into ψ_4 is also negligible because

(21) Stockis, A.; Hoffmann, R. *J. Am. Chem. Soc.* **1980**, *102*, 2952. McKinney, R. J.; Thorn, D. L.; Hoffmann, R.; Stockis, A. *J. Am. Chem. Soc.* **1981**, *103*, 2595.

(22) C–C coupling is also permitted when deviations from C_{2v} symmetry occur.[17a]

(23) (a) A small fold in the ring, as well as angular movement of the apical phosphine relative to the basal ligands does not alter the general bonding picture. (b) Hofmann, P.; Hämmerle, M.; Unfried, G. *New J. Chem.* **1991**, *15*, 769.

(24) Subscripts "s" and "a" are respectively symmetric and antisymmetric with respect to the xz plane.

of their small (δ) overlap (0.045) and large energy difference. The three occupied orbitals of the metal ($1a_1$, $1e_a$, $1e_s$) are mostly involved in four-electron destabilizing interactions with the occupied orbitals of the $C_4H_4^{2-}$ ligand and do not contribute to the stability of the complex. These orbitals will, however, play an important role in determining the reactivity of **8b**.

In consequence, although we cannot neglect the π character of the metallacycle, the small values of the Ir–C π bond indices (0.04) and the weak π-type electron transfer (0.14 electrons) between the two fragments suggest that it is not very pronounced. Thorn and Hoffmann commented on the weak π-conjugation in saturated $Rh^{III}L_4(C_4H_4)$,[10] and the absence of one ligand L in our complex does not seem to cause a significant increase in π-conjugation.

It thus begins to appear that $P_3Ir(C_4H_4)^+$ has the orbital structure appropriate for an intermediate in the cyclotrimerization reaction. We have previously demonstrated that donation from the $\pi_\perp$ orbital to the metal was central to the stability of the alkyne complex $P_3Ir(C_2H_2)^+$ (**4**); there is much less π donation (0.03 vs 0.14 electrons) in the metallacyclopentadiene. This should lead to noticeable differences in the reactivity toward an incoming ligand. It is also of interest to include the metallabenzene ring $P_3Ir(C_5R_5)$[11] in the comparison. The alkyne complex $P_3Ir(C_2R_2)^+$ is reactive toward Lewis bases but may be isolated in the absence of such reagents;[3] $P_3Ir(C_4R_4)^+$ has not been isolated in the absence of a trapping ligand. In contrast, $P_3Ir(C_5R_5)$ shows no marked reactivity toward Lewis bases.[11] A comparison of the energy of the LUMO is indicative in this case.

The LUMO energies for these three metallacycles are in the order $P_3Ir(C_4H_4)^+$ (–10.27 eV), $P_3Ir(C_2H_2)^+$ (–9.70 eV), $P_3Ir(C_5R_5)$ (–9.31 eV), which is in excellent agreement with the ordering of their reactivities toward Lewis bases. The LUMOs are derived predominantly from the interaction of the P_3Ir^{3+} $2e_s$ orbital with the closest π orbital of the carbon fragment which is symmetrical with respect to the xz plane. The low-lying LUMO of $P_3Ir(C_4H_4)^+$, **9**, is

9 **10**

mainly the in-phase combination of $2e_s$ with the empty $C_4H_4^{2-}$ ψ_3 (the occupied ψ_1 has a very weak influence), has bonding character, and is low-lying. The higher lying LUMO of $P_3Ir(C_2H_2)^+$, **5**, is the out-of-phase combination of $2e_s$ and the acetylene $\pi_\perp$, which has a destabilizing effect on the LUMO. Finally, the highest LUMO, **10**, of $P_3Ir(C_5R_5)$ is the out-of-phase combination of $2e_s$ with ψ_3, the HOMO of $C_5H_5^{3-}$. The relationship between the energy of the LUMO and the degree of unsaturation of the metal can be derived from the above description. In $P_3Ir(C_4H_4)^+$, there is very little electron transfer from ψ_1 into $2e_s$ and the electron count at the metal is close to 16. In $P_3Ir(C_2H_2)^+$, the electron transfer from $\pi_\perp$ is larger and the electron count at the metal can be viewed as intermediate between 16 and 18. In $P_3Ir(C_5H_5$, the electron transfer from the HOMO of $C_5H_5^{3-}$ is large and the electron count at the metal is close to 18.

Chart 1

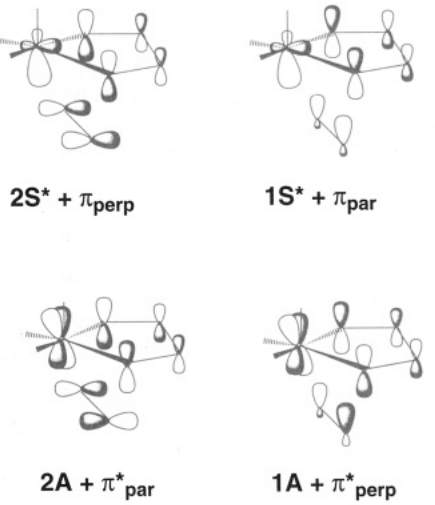

We have thus shown that the IrC_4 unit in the $P_3Ir(C_4H_4)^+$ intermediate has a planar ring structure. It is a 16-electron (Lewis-acidic) species, and the metal is only slightly stabilized by a small π donation from the conjugated carbon chain. Thus, the complex is better represented by **11b**. Such small conjugation fails to permit isolation and characterization, yet it may be sufficient for the complex to serve as a reactive intermediate.

a **b**

11

C. Reactivity of Metallacyclopentadiene. The reactivity of **8b** with respect to an incoming ligand can be analyzed using a frontier orbital approach. The presence of a low-lying metal-centered LUMO, **9**, accounts for the addition of a monodentate ligand (e.g., Cl^-) at the metal. If the incoming ligand is an acetylene, the addition reaction is facilitated provided that there is a proper symmetry match between the frontier orbitals of the two reactants. The four frontier orbitals of **8b** are the two occupied in-phase orbitals (1A) and out-of-phase (2A, HOMO of π character) combinations of ψ_2 and $1e_a$ and the two vacant in-phase (1S*, LUMO, already shown as **9**) and out-of-phase (2S*) combinations of $2e_s$ and ψ_3. These four frontier orbitals are delocalized on both the metal and the ligand. The four alkyne orbitals ($\pi_\parallel$, $\pi^*_\parallel$, $\pi_\perp$, $\pi^*_\perp$) are ideally adapted to overlap with the four frontier orbitals of **8b** in such a way that Ir–C and C–C bonds form in a concerted manner (Chart 1). Thus, the orbital $\pi_\parallel$ interacts with 1S*, $\pi_\perp$ with 2S*, $\pi^*_\perp$ with 2A, and $\pi^*_\parallel$ with 1A. These interactions lead to a product where the third alkyne makes up the central two carbons of an η^4-benzene ligand.

How does the presence of an additional ligand (such as Cl) prevent the addition reaction of the alkyne? This aspect of the reaction was also remarked upon in an earlier experimental study.[19a] The rhodium metallacycle becomes active in the catalytic cycle only after removal of the halide ligand. In the presence of the halide, a Diels–Alder type reaction could have been envisaged with a direct interaction between the diene (the C_4H_4 moiety) and the dienophile, followed by the displacement of Cl^- by the

alkyne. This is not as suitable, firstly because of the obvious steric problem of getting the two reactants to a bonding distance. Secondly, the orbitals are no longer well adapted to interact with an alkyne. For example, the 1S* orbital is used by the chlorine and is no longer available for an incoming reagent.

We conclude that the addition of an alkyne to the metallacycle proceeds in a concerted manner to give an η^4-benzene complex. This is the second step in the reaction mechanism in Figure 8. The reaction may be viewed as a metal-assisted Diels–Alder addition, where the metal plays an important role as a reactive center. This contrasts with the classical acid catalyzed Diels–Alder addition where the only role of the electrophile is to activate the diene, but not to form bonds to the dienophile.

η^4-Benzene Complex. A. Structure of the η^4-Benzene Complex. In the complex $P_3Ir(C_6H_6)^+$, schematically shown in **12**, the benzene ligand is η^4-coordinated and thus resembles, in many aspects, a diene

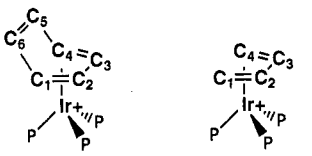

12

13

complex. The terminal C(1)–C(2) and C(3)–C(4) bonds are elongated, and the central C(2)–C(3) bond is shortened. The conformation of the IrP_3^+ is also typical of diene complexes with one Ir–P bond below the mouth of the diene. In fact, the changes in bond lengths are considerably larger than those found in η^4-diene complexes, **13**, where an equalization of the three carbon–carbon bond lengths is generally observed. In the experimental η^4-benzene complex, these changes are accentuated, as the central C–C bond (1.37 Å) is considerably shorter than the terminal C–C bonds (1.49 Å). Similar features have been observed in other η^4-benzene complexes.[25]

Two factors are responsible for the unusual C–C bond lengths in a bound η^4-arene. First, *fac*-P_3Ir^+ is a potent electron donor[3b] and the empty orbitals of the conjugated ligand accept considerable electron density. In the diene complex, **13**, the back-donation from the metal populates the diene LUMO (ψ_3) which is antibonding between the terminal carbons (C(1)–C(2) and C(3)–C(4)) and bonding between the two central (C(2)–C(3)) carbons.

The second factor controlling the C–C bond lengths in η^4-arene complexes is related to the fact that the coordinated arene is no longer planar. The folding at C(1) and C(4) diminishes the π overlap between C(1) (C(4)) and C(2) (C(3)). We have simulated this effect by calculating the C–C bond orders in the free and coordinated butadiene using both planar and distorted structures (Table 4). In Table 4, these results are compared to the free and coordinated η^4-benzene. It appears that the folding of the butadiene also weakens C(1)–C(2) and strengthens C(2)–C(3). Coordination to the metal fragment augments this effect until the C(1)–C(2) (C(3)–C(4)) bond orders are larger than that of C(2)–C(3). The observed C–C bond lengths in (tripod)$Ir(\eta^4$-$C_6H_6)^+$ are thus due to the combined effect of the potent electron-donating capacity of the Ir(I) center and the distortion of the benzene, which changes the hybridization at the C(1) and C(4) carbons. These features make the benzene a stronger electron acceptor than butadiene itself.

Table 4. Mulliken Overlap Population for the C–C Bonds in Butadiene and Benzene[a]

diene	bond	planar C_4H_6	dist C_4H_6[b]	η^4-C_6H_6
free	C(1)–C(2)	1.18	1.15	1.01
	C(2)–C(3)	0.95	0.97	1.11
complex[a]	C(1)–C(2)	1.00	0.97	0.95
	C(2)–C(3)	1.04	1.06	1.10

[a] All C–C bond lengths are equal to 1.4 Å to permit direct comparison. [b] The two endo H of the terminal C(1) and C(4) of butadiene are out of the plane of butadiene and are positioned along the C(1)–C(6) and C(4)–C(5) directions, as in the experimental η^4-benzene complex. [c] Coordinated to $Ir(PH_3)_3^+$.

B. Fluxionality of the η^4-Benzene Complex. How do all six benzene hydrogens, all six benzene carbons, and all three phosphines become time-average equivalent? We showed above that this process occurs without Ir–P bond cleavage and that a single activation energy governs both P and ring hydrogen fluxionality. We therefore now explore all plausible structures for the coordination of benzene to an intact $[IrP_3]^+$ fragment. We shall see how what begins as a study of fluxionality will also explain the benzene-release step in the cyclotrimerization reaction.

Our approach to this problem is to analyze the different binding modes of $[IrP_3]^+$ to benzene. We have chosen to dissect the problem into two parts: (i) the flattening of the bent η^4-coordinated benzene and (ii) the torsional and migrational motion of $[IrP_3]^+$ over a planar benzene. We assume that no dissociation of a phosphine occurs during this process. This dissection of the problem limits the degrees of freedom to a manageable number. However, this approach is chemically reasonable because there is a thermodynamic preference for a planar benzene and because it maintains a maximum use of metal d orbitals (i.e., number of Ir/C contacts).

(a) The Unlikelihood of (η^6-benzene)IrP_3^+. The [(η^6-benzene)$IrP_3]^+$, **14**, is a 20-electron complex and is therefore highly unstable. The orbital pattern of an (η^6-

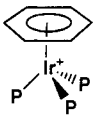

14

benzene)ML_3 is well-known.[26] The HOMO of **14** is one component of the degenerate pair arising from the antibonding combination of the 2e″ benzene orbitals with the 1e set of the IrP_3^+ fragment. The system should therefore be a spin triplet, but there is no evidence of paramagnetic species during the catalytic cycle, which suggests that a more stable diamagnetic intermediate exists. Jahn-Teller distortion of **14** provides some reasonable alternative structures which retain a planar benzene ring and are now evaluated as a mechanism for fluxionality.

(b) Site Exchange between the Planar Benzene Carbons. The energy variation for the movement of the $[IrP_3]^+$ fragment over a planar benzene ring at a fixed

(25) (a) Huttner, G.; Lange, S. *Acta Crystallogr.* **1972**, *B28*, 2049. (b) Muetterties, E. L.; Bleeke, J. R.; Wucherer, J. R.; Albright, T. A. *Chem. Rev.* **1982**, *82*, 499 and references therein.

(26) Albright, T. A.; Burdett, J. K.; Whangbo, M.-H. *Orbital Interactions in Chemistry*; Wiley: New York, 1985.

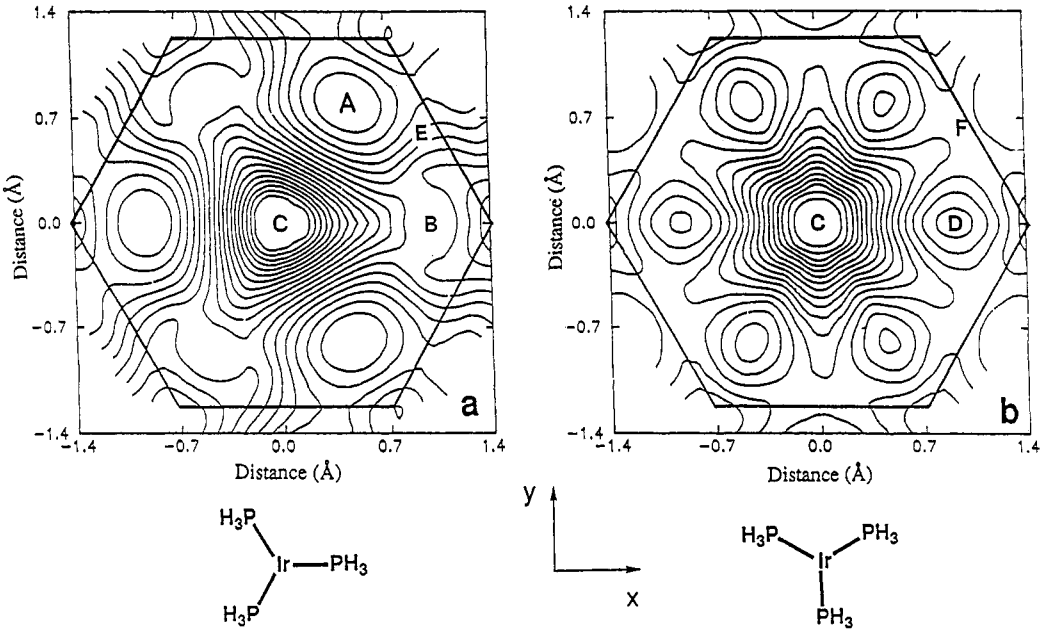

Figure 12. Potential energy surfaces for movement of $(PH_3)_3Ir^+$ below the plane of the benzene surface. The distance between Ir and the benzene plane is equal to 1.9 Å. Energy levels are separated by 2 kcal/mol. For surface a, one Ir–P bond is kept parallel to the x axis. For surface b, one Ir–P bond is kept parallel to the y axis.

Ir/plane distance is represented by the two potential energy surfaces a and b (Figure 12). Each energy surface was calculated by allowing the metal to move over the ring without any rotation of the phosphines.

On surface a, one of the Ir–P bonds points away from the benzene ring center when θ (the rotation angle of one Ir–P bond projection with respect to the x axis) = 0, 120, and −120° and toward the center of the ring when θ = 60, 180, and −60°. On surface b, one of the Ir–P bonds bisects a benzene edge either away from or toward the center when $\theta = (30° + n60°)$. The two surfaces, plotted using a common reference energy, permit a complete analysis of the haptotropic shift of the metal fragment which *includes* the rotation of the phosphines about the metal–benzene vector.

There are a number of important positions on each surface which require discussion. On both surfaces, the η^6 structure, **14**, is calculated to be a maximum (point C) which means that the migration of the $[IrP_3]^+$ fragment must occur without ever passing over the benzene ring center (a Jahn–Teller unstable structure). The absolute minimum on surface a is found at A (θ = 60°) and all the energies are quoted relative to this point. There is a secondary minimum at B (θ = 0°) at 12 kcal/mol. The minimum on surface b is at D (5 kcal/mol). The point F on surface b (just outside the ring) will also be important (10 kcal/mol). This region of space on surface a which has almost the same energy as F is called E.

The difference between A, D, and B corresponds to rotation by 30 or 60° of the IrP_3 group around its C_3 axis. At these points, the metal is close to three carbon centers and can be viewed as containing the η^3-coordinated benzene complex. At E and F, which differ by a 30° rotation of IrP_3, the complex can be recognized as containing η^2-coordinated benzene. Rotation of the olefin is clearly a low-energy process for this latter structure.

The fluxional process requires movement of the metal over the ring (change in θ) combined with a rotation of the IrP_3 group with respect to the edges of the ring. Our energy surfaces lead to a description of the fluxional process as a "waltz". Starting at the minimum A, the complex moves to E. At E, the rotation of the IrP_3 group is a low-energy process and it may rotate by 60°, via F (thus surface a → surface b). The complex may then continue on surface b to a point which is B in terms of θ, but now the IrP_3 group has rotated by 60° and B has become an A point. This waltz continues, alternating between an A structure, where the metal is close to one apex of the hexagon, and an F structure, where the metal is close to the middle of an edge. The waltz is accompanied by rotation of IrP_3 such that at each A point, an Ir–P bond points toward the center of the ring. In this process, all six carbons and all three phosphorus atoms become equivalent, without ever passing through the central (η^6) structure, C. The calculated energy cost of this migration is 12 kcal/mol.

This potential energy surface shows two structures which are low in energy and are best described as η^3- and η^2-coordinated benzene. It is remarkable that the η^4 structure is not a minimum. The reason is that it could only exist with a strong distortion away from planarity of the benzene ring. Similar distortions are actually required to stabilize the η^2 structure (**15**). It should also be pointed out that although the site exchange process requires the six-membered ring to be more planar than in the η^4 structure, total planarity need not be achieved. Our conclusions would not be affected by some folding of the ring during the metal migration. It appears that the carbon and phosphine exchange is a facile reaction. Unfortunately, EHT calculations do not readily permit more quantitative analysis of the exchange process.

Despite the planar ring constraint, these η^3 and η^2 structures have clear relationship with isolable related species. However, their molecular orbital scheme shows the presence of small HOMO–LUMO gaps. These species will not be isolated and are at best short-lived species.

(c) The Allyl Structure (η^3-Benzene)IrP_3^+. In the (η^3-benzene)IrP_3^+ species, the bonding of the three carbons to iridium resembles that of an allylic species. An η^3-coordination mode would polarize the benzene π orbitals in a (C_3^+,C_3^-) manner, with the negatively charged part

bonded to the metal. Although this polarization is unlikely in free substituted benzene, such a structure may be still a reactive intermediate, provided that it is stabilized by the metal fragment. The preferred orientation of the three phosphines with one Ir–P bond below the open mouth of the allyl fragment (A) is also that observed in a d^8 ML_3-(allyl) complex.[27]

(d) The η^2-Benzene Complex. The (η^2-benzene)IrP_3^+ species (with nonhybridized coordinated carbons or hybridized carbon like in **15**) is very reactive because the

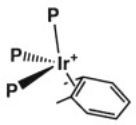

15

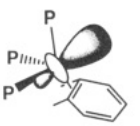

16

η^2-benzene gives only the two electrons of the coordinated double bond. The low-lying LUMO **16** is ideally suited for interacting with an incoming ligand. Therefore, unlike the d^8 P_3Ir(alkyne)$^+$ complex in which the alkyne is acting as a 4-electron donor, the 16-electron η^2-benzene complex can only be isolated with an additional ligand to the metal like in CpML(η^2-benzene).[28] The rotation of the benzene ligand is energetically easy for the same reasons that rotation of alkyne is easy in the P_3Ir(alkyne)$^+$ complexes.[3b]

In conclusion, the energetically easy waltz of the metal fragment under the benzene ring as well as its rotation around its own C_3 axis is the suggested route for the observed fluxional process.

(e) Alternative Mechanisms for Fluxionality. An alternative approach might be to consider the rearrangement to an η^2-metallanorbornadiene form, **17**. Passage

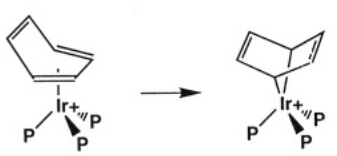

17

through this structure does not exchange all carbons,[29] and other structural reorganizations would be required if this intermediate were on the reaction path. Reaching the metallanorbornadiene structure implies an oxidation process at the metal. EHT calculations disfavor this intermediate by 70 kcal/mol, and although such a value should be treated with caution, it suggests that the metallanorbornadiene is an unlikely intermediate.

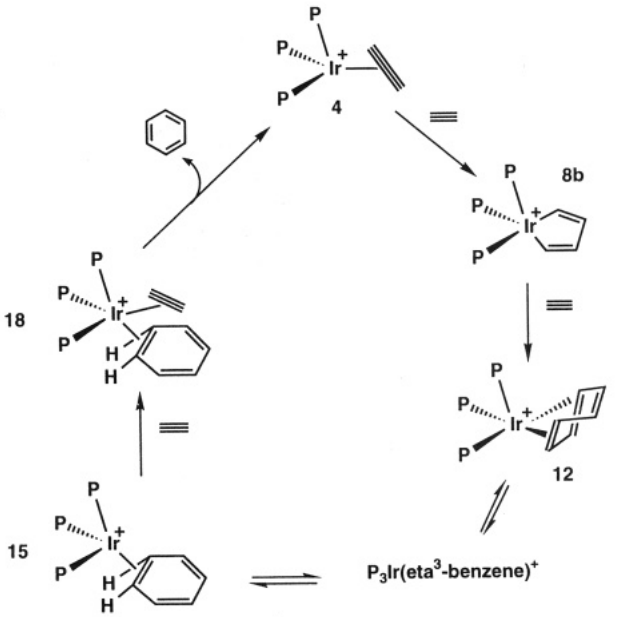

Figure 13. Representation of the catalytic reaction path for alkyne cyclotrimerization showing the relationship between the fluxionality of the η^4-benzene ligand and the catalytic reaction.

(f) Reactivity of the η^4-Benzene Complex. The benzene ring of the η^4-benzene complex, **1**, reacts with hydride to form a C–H bond and a σ-allyl complex.[30] Since butadiene complexes do not react under similar conditions, we can assume that this addition does not occur in the ground state of the complex. The experiment was performed at a temperature where fluxionality is rapid, and from our interpretation of this process, we can propose two intermediates on the potential energy surface that may favor such an addition reaction. One of these is the η^3-benzene complex, which has a polarization of the benzene π cloud such that some of the benzene carbons are electrophilic. This favors direct addition to the ring *anti* to the metal. *The second is the η^2 complex, which has a vacant site at the metal, making it very reactive toward nucleophilic attack and addition syn to the metal.* While the experimental results do not allow us to distinguish between the two processes, the proposed exchange mechanism is clearly in full agreement with the reactivity of the complex.

(g) Relationship between the Site Exchange and Catalytic Processes. A scheme showing both the exchange and catalytic processes is given in Figure 13. Flattening the benzene ring from its ground state η^4-coordination, **12**, results in a displacement of the metal away from its center toward an η^3-coordination mode. Rotation of the IrP_3 fragment about its local C_3 axis is achieved via an η^2-coordination mode. In the absence of an external reagent, the η^2 complex will convert into a different η^3 complex, which may return to the η^4 ground state structure or may continue to move over the benzene ring.

In the presence of a new reagent, the very low-lying LUMO of the η^2 complex, **15**, facilitates coordination of the reagent to give **18**. If this reagent is an alkyne (which can serve as a 4-electron donor), the metal becomes too rich in electrons and one of the two ligands is forced to

(27) Albright, T. A.; Hofmann, P.; Hoffmann, R. *J. Am. Chem. Soc.* **1977**, *99*, 7546.

(28) (a) Browning, J.; Green, M.; Penfold, B. R.; Spencer, J. L.; Stone, F. G. A. *J. Chem. Soc., Chem. Commun.* **1973**, *31*. (b) Browning, J.; Penfold, J. R. *J. Cryst. Mol. Struct.* **1974**, *4*, 335. (c) Browning, J.; Green, M.; Spencer, J. L.; Stone, F. G. A. *J. Chem. Soc., Dalton Trans.* **1974**, 97. (d) Silverthron, W. E. *Adv. Organomet. Chem.* **1975**, *13*, 48. (e) Brauer, D. J.; Krüger, C. *Inorg. Chem.* **1977**, *16*, 884. (f) Cobbledick, R. E.; Einstein, F. W. B. *Acta Crystallogr.* **1978**, *B34*, 1849. (g) Heidjen, H.; Orpen, A. G.; Pasman, P. *J. Chem. Soc., Chem. Commun.* **1985**, 1576. (h) Harman, W. D.; Sekine, M.; Taube, H. *J. Am. Chem. Soc.* **1988**, *110*, 5725. (i) Belt, S. T.; Duckett, S. B.; Helliwell, M.; Perutz, R. N. *J. Chem. Soc., Chem. Commun.* **1989**, 928. (j) Jones, W. D.; Dong, L. *J. Am. Chem. Soc.* **1989**, *111*, 8722. (k) Belt, S. T.; Helliwell, M.; Jones, W. D.; Partridge, M.; Perutz, R. N. *J. Am. Chem. Soc.* **1993**, *115*, 1429.

(29) It generates only a time-averaged mirror plane perpendicular to the ring, but not a C_6 axis.

(30) Bianchini, C.; Caulton, K. G.; Folting, K.; Meli, A.; Peruzzini, M.; Polo, A.; Vizza, F. *J. Am. Chem. Soc.* **1992**, *114*, 7290.

leave. The departure of the benzene is thermodynamically favorable because an uncoordinated benzene will recover its aromaticity and $IrP_3(alkyne)^+$ complexes, **4**, are detectable species. The catalytic cycle can thus continue. Thus, since the fluxionality involves a decrease in hapticity of the C_6H_6 ligand, it naturally furnishes a path for *displacement* of the benzene product by the incoming monomer (alkyne).

Why is the catalytic cycle efficient? None of the intermediates species are "pure" 16-electron species, being more or less enriched by donation from the π systems of the carbon chains. However, they all have a low-lying LUMO and are reactive toward an incoming reagent. It is important that the metallic fragment has a *fac* (pyramidal) ML_3 geometry because this prevents the system from falling in the stable trigonal bipyramidal bis(alkyne) well, which is a dead end for the C–C coupling reaction. Similarly, the coordinated benzene complex should not be highly stable; otherwise the reaction would be stoichiometric and not catalytic. This aspect of the reaction has been examined by Chaudret *et al.*,[31] who treated $[CpRu(OMe)]_2$ in the presence of acetylene and CF_3SO_3H in CH_2Cl_2. This yields a stoichiometric amount of stable $CpRu(\eta^6\text{-benzene})^+$. Since $CpRu(\eta^6\text{-benzene})^+$ is a stable 18-electron species, it has no driving force to partially decoordinate the benzene ligand. This reduces the chances of a new acetylene molecule to coordinate and stops the catalytic cycle. The (tripod)Ir^I or (tripod)Rh^I fragments, with two additional electrons relative to $CpRu^+$, have all the requirements to be efficient catalysts for alkyne cyclotrimerization.

(31) See: Carreno, R.; Chaudret, B.; Labrove, D.; Sabo-Etienne, S. *Organometallics* **1993**, *12*, 13 and references therein.

Acknowledgment. C.B. is indebted to Progetti Finalizzati "Chimica Fine II", CNR, Rome, Italy. This work was also supported by the U.S. NSF (Grants CHE-9103915 and INT-88-14838), by the NSF/CNRS grant for U.S./France scientific collaboration, and by the Indiana University Institute for Advanced Study (fellowships to O.E. and to C.B.). The Laboratoire de Chimie Théorique is associated with the CNRS (URA 506).

Supplementary Material Available: Tables of full crystallographic details and anisotropic thermal parameters for [(triphos)Ir(C_6H_6)](BPh_4) (3 pages). See any current masthead page for ordering information.

OM9306990